JOURNAL OF APPLIED POLYMER SCIENCE VOL. 11, PP. 251-287 (1967)

Studies on Melt Spinning. II. Steady-State and Transient Solutions of Fundamental Equations Compared with Experimental Results

SUSUMU KASE and TATSUKI MATSUO, *Toyobo Co., Ltd., Kitaku, Osaka, Japan*

Synopsis

In the part installment of the present paper, the authors formulated the dynamics of melt spinning by introducing a set of fundamental equations that consist of the equations of heat, force, and material balances. Some steady-state solutions were also given. Additional steady-state solutions corresponding to many different spinning conditions for polyester and polypropylene filament yarns consistently show good agreement with experimental results. These steady-state solutions that give filament cross-section $A(x)$ and filament temperature $t(x)$ as functions of position x are correlated with yarn qualities: yarn density and birefringence, crystallinity and molecular orientation, are correlated respectively with the speed of polymer cooling at 100°C. and the maximum tensile stress $(F/A)_w$ acting on the filament. A transient solution of the fundamental equations computed on an IBM 1401 machine shows that the filament cross-section A at the take-up roll forms a large transient peak after a stepwise increase in the speed v_y of cooling air. This agrees with experiments fairly well. The fundamental equations, therefore, clarify the dynamic relations between cooling air speed and yarn weight variations.

INTRODUCTION

As discussed in the previous paper,[1] fundamental eqs. (1), (2), and (3) are mathematical formulations of the dynamics of melt spinning; these are, respectively, equations of heat, force, and material balances.

$$v(\partial t/\partial x) + (\partial t/\partial \tau) = -(2\sqrt{\pi}h/\sqrt{A}\rho C_p)(t - t^*) \quad (1)$$

$$(\partial v/\partial x) = (F/\beta A) \quad (2)$$

$$v(\partial A/\partial x) + (\partial A/\partial \tau) = -A(\partial v/\partial x) \quad (3)$$

In these equations, position x (in centimeters) measured from the spinneret and time τ (in seconds) are the independent variables; temperature t (°C.) filament velocity v (in centimeters/second) and the cross-sectional area A (in square centimeters) of the filament are the dependent variables. t^* is the temperature of the surrounding air; h (in calories per square centimeter per degree per second) is the coefficient of heat transfer at the filament surface. The melt-spinning system is diagrammed in Figure 1.

Equations (1), (2), and (3) are introduced under the assumptions that (*1*) filaments are circular in cross-section; (*2*) temperature t is uniform across a filament cross-section; (*3*) heat conduction within the filament in the x direction is negligible; (*4*) swelling of the polymer stream at the nozzle exit, the Barus effect, is disregarded; (*5*) tensile viscosity β of the polymer is dependent only on temperature t; (6) filament tension F is in general a function of time τ but is independent of position x.

In the present paper, eqs. (1), (2), and (3) are solved for a number of steady-state solutions corresponding to different spinning conditions;

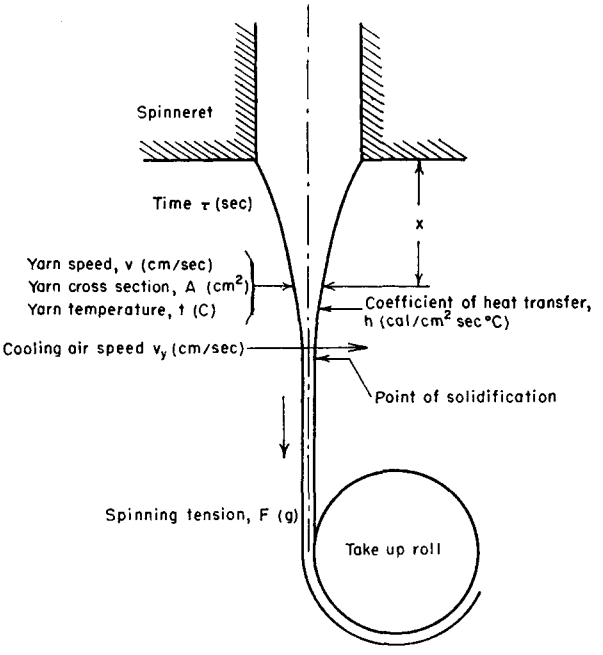

Fig. 1. Melt-spinning system.

these solutions are then compared with experimental results to demonstrate their agreement; the yarn qualities, density, and birefringence, are correlated with the steady-state solutions; a transient solution corresponding to an abrupt change in the speed v_y of cooling air is machine computed and compared with experimentally measured values.

Subsequent sections discuss the coefficient h of heat transfer and the properties tensile viscosity β, density ρ, and isobaric specific heat C_p of polypropylene as prerequisites to the solution of the fundamental equations.

We wish to note that the mathematical expression of h in the present paper is slightly different from the one in the previous paper. The change is made for the purpose of rigorousness.

COEFFICIENT OF HEAT TRANSFER h

In the previous paper, the coefficient h of heat transfer for a fine cylindrical filament cooled by an air current was given as

$$\mathrm{Nu} = 0.42\ \mathrm{Re}^{0.334}(1 + K) \tag{4}$$

where

$$\mathrm{Nu} = (hd/k_F) = (2h/k_F)\sqrt{A/\pi} \tag{5}$$

and

$$\mathrm{Re} = (vd/\nu_F) = (2v/\nu_F)\sqrt{A/\pi} \tag{6}$$

In eqs. (5) and (6), k_F and ν_F are, respectively, the heat conductivity and kinematic viscosity of air, and d is the diameter of filament.

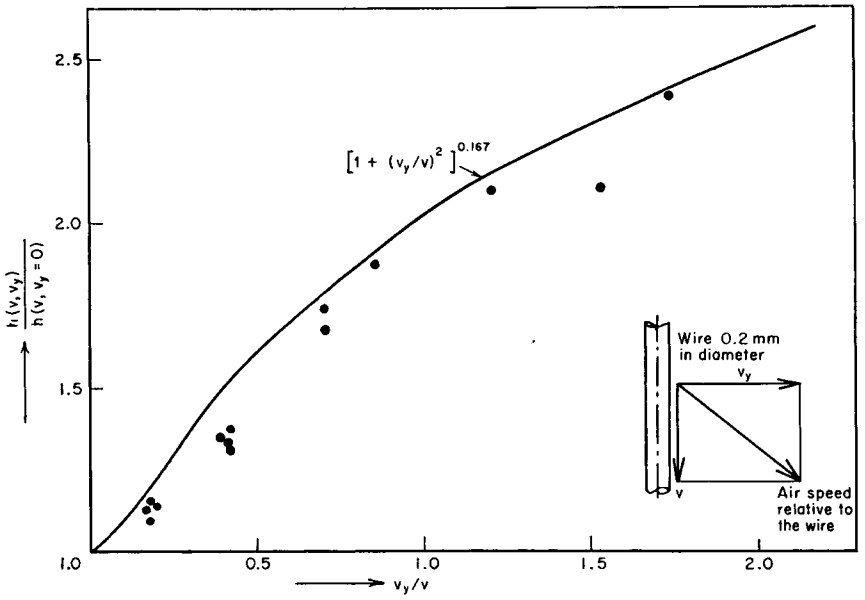

Fig. 2. Changes in the coefficient h of heat transfer with changes in the v_y component of air speed. The v component is kept unchanged.

The coefficient $(1 + K)$ expresses the effect of the direction angle of the air current measured from the filament axis. K is equal to zero when the air current is parallel to the filament and is approximately unity when the air current is at right angles to the filament. To be exact, K should be expressed as an explicit function of the direction angle rather than given as a constant. Experiments reveal that K is related to the tangent v_y/v of the direction angle as shown in Figure 2, provided the value of v is kept constant. (Figure 2 is identical to Figure 6 of Part I). Here v is the speed of the filament running in the vertical direction and v_y is the speed of cooling

air flowing in the horizontal direction. v_y/v is, therefore, the tangent of the angle formed by the air current and the wire axis.

Equation (7) approximately fits the experimental relation in Figure 2.

$$1 + K = [1 + (8v_y/v)^2]^{0.167} \tag{7}$$

By introducing eqs. (5), (6), and (7) into eq. (4), one obtains

$$h = 0.388(k_F\nu_F^{-0.334})A^{-0.334}v^{0.334}[1 + (8v_y/v)^2]^{0.167} \tag{8}$$

Equation (8) is the most generalized expression for the coefficient h of heat transfer for air flowing past a fine cylindrical filament at different angles to its axis. The factor $(k_F\nu_F^{-0.334})$ consisting of physical properties of air is approximately constant

$$(k_F\nu_F^{-0.334}) = 1.22 \times 10^{-4} \tag{9}$$

over the range of temperatures encountered in most melt spinning. Equation (8), therefore, simplifies to

$$h = 0.473 \times 10^{-4}A^{-0.334}[v^2 + (8v_y)^2]^{0.167} \tag{10}$$

Equation (10) is valid regardless of polymer type, for e.g., nylon, polyester, or polypropylene, as long as the filament cross-section is approximately circular.

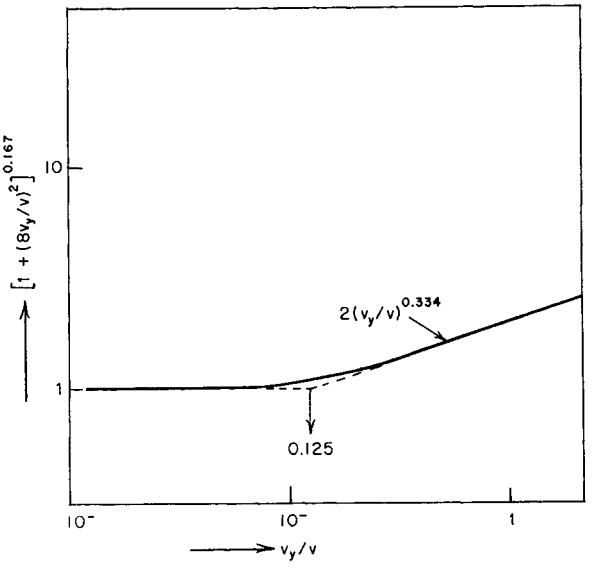

Fig. 3. Logarithmic plot of $[1 + (8v_y/v)^2]^{0.167}$ vs. v_y/v.

Equation (10) agrees with the literature,[1–5] in that the value of h for cross flow ($v = 0$, $v_y = a$) is about twice as large as that for parallel flow ($v = a$, $v_y = 0$).

The right-hand side of eq. (7), $[1 + (8v_y/v)^2]^{0.167}$, has an interesting characteristic worth commenting on. In Figure 3 $[1 + (8v_y/v)^2]^{0.167}$ is clotted against v_y/v on log–log graph paper. Figure 3 shows that as a first approximation

$$[1 + (8v_y/v)^2]^{0.167} = 1 \qquad v_y/v < 0.125 \qquad (11)$$

and

$$[1 + (8v_y/v)^2]^{0.167} = 2(v_y/v)^{0.334} \qquad v_y/v > 0.125 \qquad (12)$$

or, in other words, with reference to eq. (10),

$$[v^2 + (8v_y)^2]^{0.167} = v^{0.334} \qquad v_y/v < 0.125 \qquad (13)$$

and

$$[v^2 + (8v_y)^2]^{0.167} = 2v_y^{0.334} \qquad v_y/v > 0.125 \qquad (14)$$

The above relations are interpreted as follows. Suppose the speed v_y of cooling air flowing in the horizontal direction is constant over the entire span of the spinning chamber. Then, at some point along the melt-spun filament, v_y/v becomes equal to 0.125, because yarn speed v is usually much smaller than the air speed v_y at the spinneret and the reverse is true at the take-up roll.

$$v_y/v = 0.125 \qquad (15)$$

Above such position along the filament, the term v^2 practically disappears from eq. (10). In other words, in the upper part of the spinning chamber the cooling of the filament is governed solely by the speed v_y of cooling air flowing crosswise to the filament. In the lower part of the spinning chamber, on the other hand, the cooling is governed almost entirely by the speed v of the running filament. The position x that satisfies eq. (15) depends on many factors, but it is roughly halfway between the spinerret and the point where the filament ceases to thin.

TENSILE VISCOSITY β, DENSITY ρ, AND SPECIFIC HEAT C_p OF POLYPROPYLENE

The tensile viscosity β defined by eq. (2) is identical in dimension to the usual coefficient of viscosity for fluids.[1] β is known to depend on such factors as polymer type, intrinsic viscosity $[\eta]$, temperature t, rate of deformation dv/dx, etc. Throughout this study, effects of dv/dx are disregarded as negligible, and β is assumed a function only of temperature t for a specified polymer type and $[\eta]$.

Values of $\beta(t)$ for polypropylene are deduced[1] from experimentally measured $A(x)$ and $t(x)$ values by using eqs. (2) and (3) and are plotted semilogarithmically against $1000/(t + 273)$ as shown in Figure 4. The experimentally measured $A(x)$ and $t(x)$ values used in deriving the

$\beta(t)$ are those shown in Figures 7–10. Polypropylene pellets used in these experiments had an intrinsic viscosity of 1.10 (135°C., Tetralin).

Equation (16) expresses the straight line portion of curve A in Figure 4:

$$\beta = 0.040e^{3500/(t+273)} \tag{16}$$

The $\beta(t)$ curve is expected to deviate from linearity at about 70°C., bend sharply upward, and ultimately reach infinity, because the experimental $A(x)$ and $t(x)$ values show that filaments practically cease to thin at about 70°C. Since it is difficult to determine $\beta(t)$ in the temperature range below 70°C., the right upper portion of curve A in Figure 4 is drawn arbitrarily.

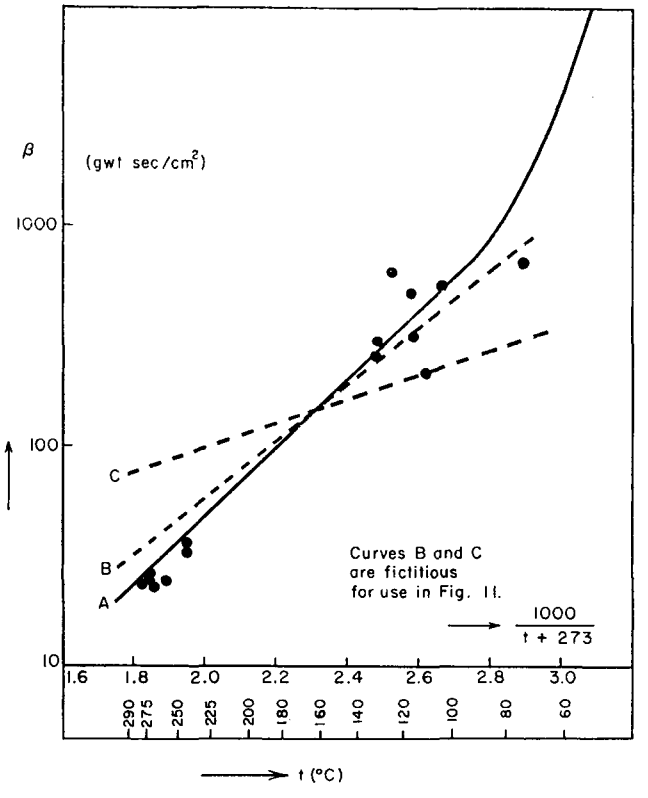

Fig. 4. Tensile viscosity β vs. reciprocal absolute temperature, $1000/(t + 273)$.

However, this particular curve is used consistently in all computations involving polypropylene. The exponent in eq. (16) shows that the activation energy of the polymer is 7.0 kcal./mole.

Figure 5 shows the density of polypropylene determined dilatometrically. β varies both with temperature t and the extent of allowed crystallinity.

Figure 6 is the isobaric specific heat C_p of isotactic and atactic polypropylene as given by Smith and Dole.[6] In solving the fundamental eqs. (1), (2), and (3), however, both ρ and C_p are assumed constants for simplicity:

$$\rho = 0.83 \text{ g./cm.}^3$$
$$C_p = 0.70 \text{ cal./g.-deg.} \tag{17}$$

The latent heat of crystallization is disregarded as negligible.

Values of β, ρ, and C_p used in the computations for the polyester fibers are shown in Figures 9, 10, and 12 of Part I.

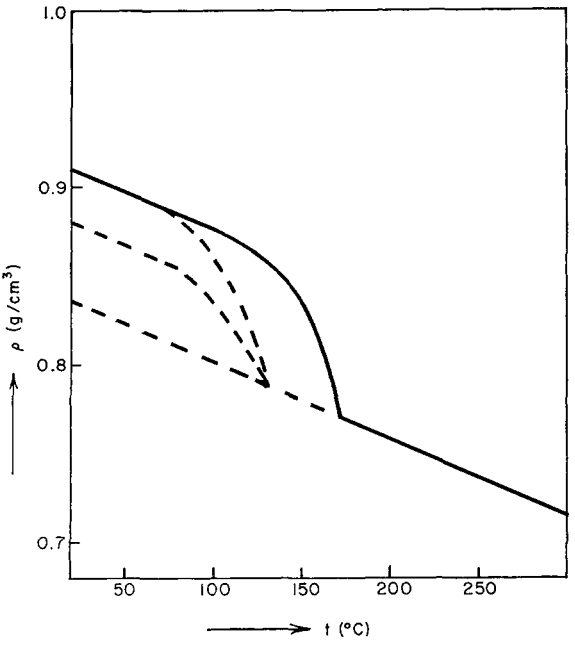

Fig. 5. Density of polypropylene vs. temperature. Crystallization affects ρ in the low-temperature range.

By introducing eq. (10) and the relation shown as curve A in Figure 4 into eqs. (1) and (2), the fundamental equations become complete and ready for solution.

$$v(\partial t/\partial x) + (\partial t/\partial \tau) = 1.67 \times 10^{-4}(1/\rho C_p)A^{-0.833}[v^2 + (8v_y)^2]^{0.167} \times (t^* - t) \tag{18}$$

$$(\partial v/\partial x) = (F/A\beta) \tag{19}$$

$$v(\partial A/\partial x) + (\partial A/\partial \tau) = -A(\partial v/\partial x) \tag{20}$$

TABLE I
Spinning Conditions for Figures 7–18

Filament type	Fig. no.	Curve No.	t_N, °C.	D_N, mm.	v_w, m./min.	t, °C.	v_y, cm./sec.	Filament denier	Notes
Polypropylene filament, yarns	7	0	240	0.6	500	20	20	8	E[b]; t_N varied
	"	1	270	"	"	"	"	"	" "
	8	2	240	"	"	"	30	"	E; t_N varied
	"	3	255	"	"	"	"	"	"
	9	4	270	"	300	"	"	"	E; v_w varied
	"	5	"	"	500	"	"	"	"
	"	6	"	"	625	"	"	"	E; "
	10	7	"	"	500	"	"	4.8	E; G varied
	"	8	"	"	"	"	"	8	"
	"	9	"	"	"	"	"	60	E; "
	11	10	"	"	"	"	"	8	β = curve *A*, Fig. 4
	"	11	"	"	"	"	"	"	" *B* "

	"	12	"	"	"	"	"	"	" C "
	12	13	"	0.4	"	"	"	"	D_N[a] varied
	"	14	"	1.6	"	"	"	"	"
	13, 14	15	"	0.8	"	"	"	"	Insulating cylinder used; t^* as given in Fig. 13.
	"	16	"	"	"	"	"	"	
	"	17	"	"	"	"	"	"	
	15	18	"	"	"	0	"	"	t^* varied
	"	19	"	"	"	50	"	"	"
	16	20	"	0.6	"	20	20	"	v_y varied
	"	21	"	"	"	"	120	"	"
Polyester filament yarns	17	22	250	0.3	600	30	0	7.5	t_N varied
	"	23	280	"	"	"	"	"	"
	18	24	"	"	"	"	"	15	G varied
	"	25	"	"	"	"	"	3.75	"

[a] D_N = nozzle diameter.

[b] E indicates that experimental data are available for comparison with theoretical curves.

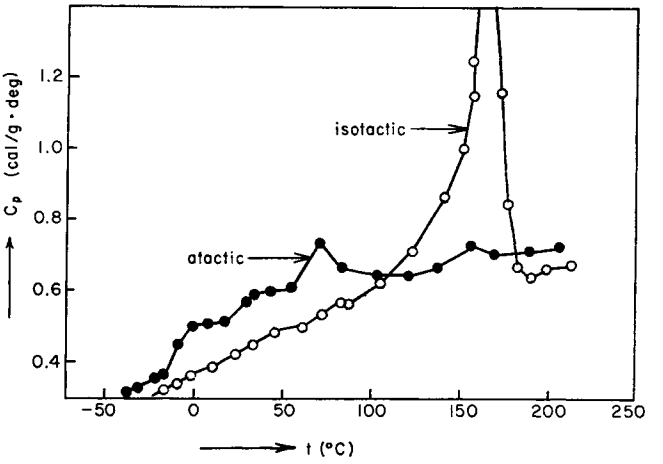

Fig. 6. Isobaric specific heat of isotactic and atactic polypropylenes as given by Smith and Dole.[6]

STEADY-STATE SOLUTIONS AND EXPERIMENTAL VALUES

In a steady state, derivatives with respect to time τ disappear from eqs. (18), (19), and (20). Equation (20) is then readily integrated to give

$$G = \rho A v \tag{21}$$

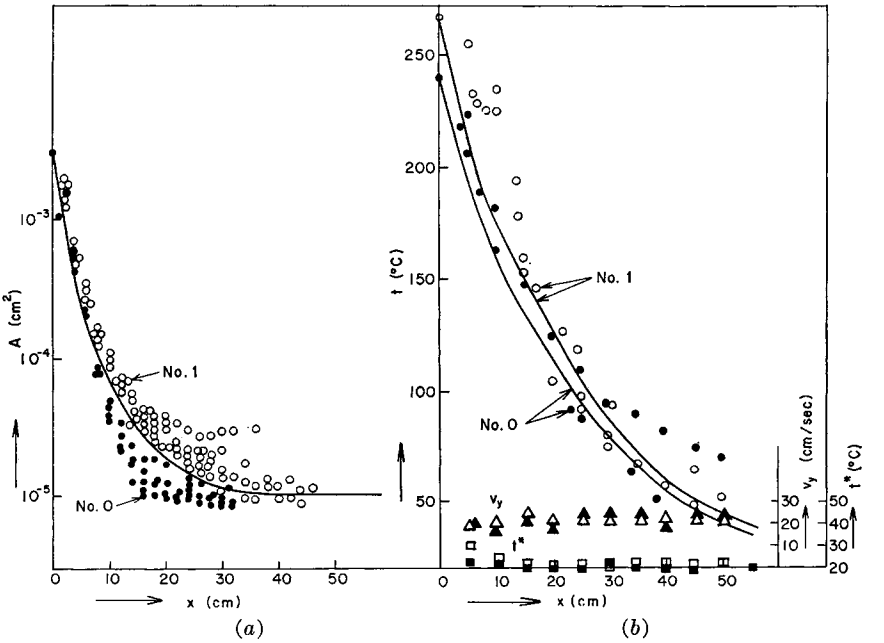

Fig. 7. Filament cross-section A, filament temperature t, air speed v_y, and air temperature t^* at different spinneret temperatures t_N: (○, ●) experimental; (——) theoretical. See Table I for other conditions.

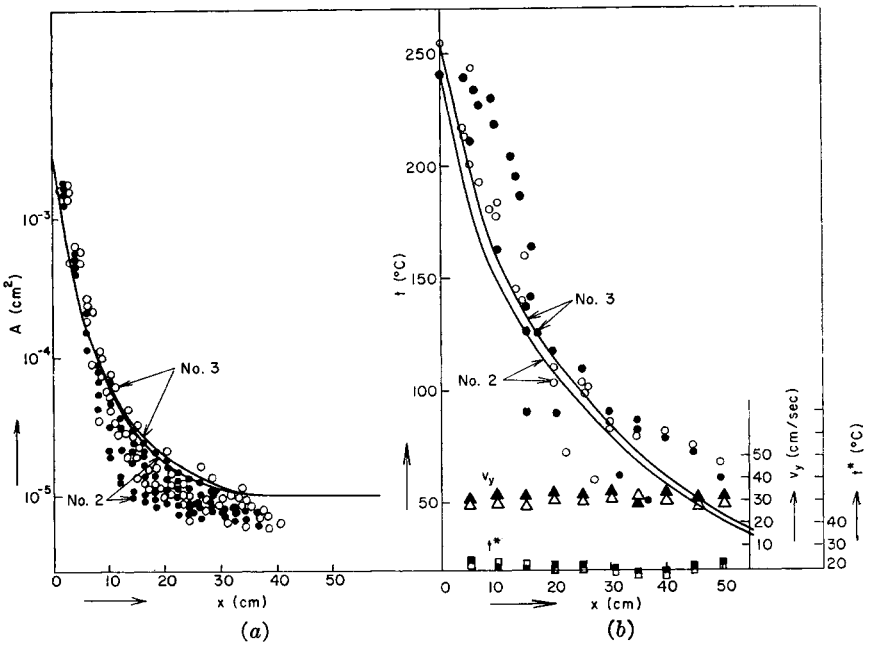

Fig. 8. Filament cross-section A, filament temperature t, air speed v_y, and air temperature t^* at different spinneret temperatures: (O, ●) experimental; (——) theoretical (calculated). See Table I.

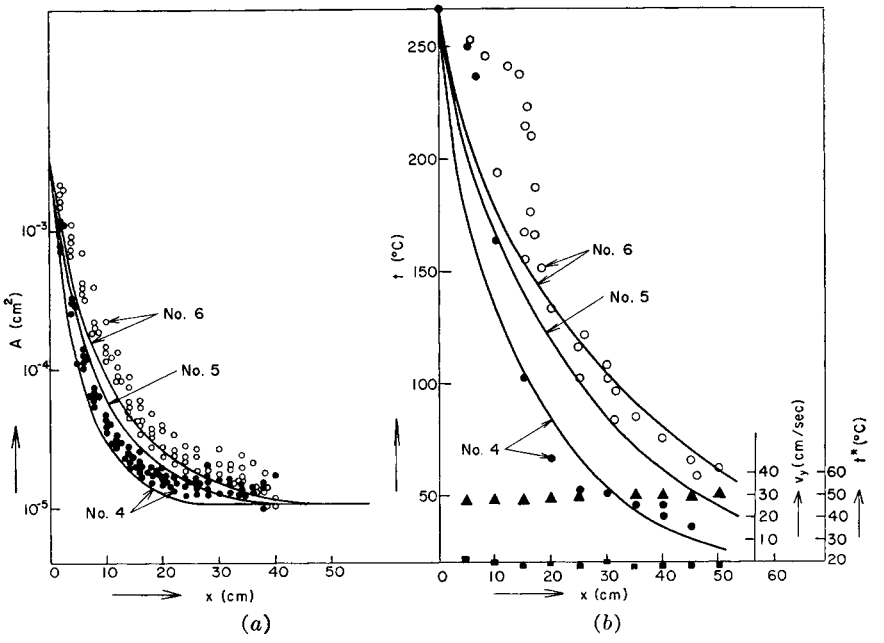

Fig. 9. Filament cross-section A, filament temperature t, air speed v_y, and air temperature t^* at different take-up speeds: (O, ●) experimental; (——) theoretical (calculated). See Table I.

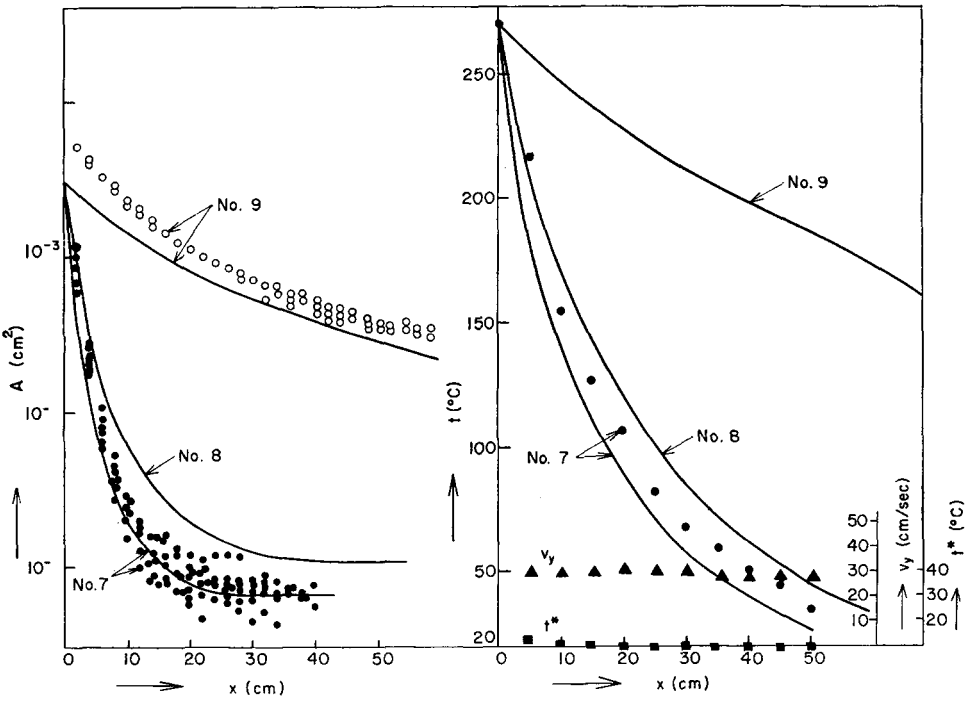

Fig. 10. $A(x)$, $t(x)$, v_y, and t at different polymer flow rates: (○, ●) experimental; (——) theoretical (calculated). See Table I.

where G (in grams per second) is the mass rate of polymer flow per filament. Introducing eq. (21) into eqs. (18) and (19), we get

$$(dt/dx) = 1.67 \times 10^{-4}\rho^{-0.334}C_p^{-1}G^{-0.666}A^{-0.167}(t^* - t) \times [1 + (8\rho A v_y/G)^2]^{0.167} \quad (22)$$

$$(dA/dx) = -(\rho F A/\beta G) \quad (23)$$

Equations (22) and (23) can be integrated by eliminating dx from them and separating the variables, provided the air speed v_y and the air temperature t^* are given as constants or as functions of A and t.

$$\int_{A_w}^{A_N} A^{-0.334}[(G/8\rho A v_y)^2 + 1]^{0.167}dA = 0.30 \times 10^4 v_y^{-0.334}F \int_{t_w}^{t_N} [(C_p\rho)/\beta(t - t^*)]dt \quad (24)$$

Subscripts N and w denote respectively the spinneret nozzle and the solidification point. Equation (24) determines the value of F, since all other values in the equation are known. Once F becomes a known quantity, eq. (24), with A_w and t_w replaced by A and t, gives $A(t)$ as a function of t.

By using this $A(t)$ relation, eq. (23) is integrated to give $A(x)$ as a function of position x. Finally, $A(x)$ is compared with $A(t)$ to yield $t(x)$.

The $A(x)$ and $t(x)$ curves shown in Figures 7–18 are solutions of eqs. (22) and (23) computed in the above manner under different spinning conditions listed in Table I. Unless an insulating cylinder is placed below the spinneret (Fig. 13), air speed v_y and air temperature t^* are approximately constant in practice as shown by the experimental points in Figures 7–10.

Figures 7–10 show experimentally measured $A(x)$ and $t(x)$ values obtained under spinning conditions identical to those for each theoretical curve. As discussed in Part I, $A(x)$ is measured by trapping the molten filament in a booklike instrument and the $t(x)$ is measured by means of a special thermocouple.

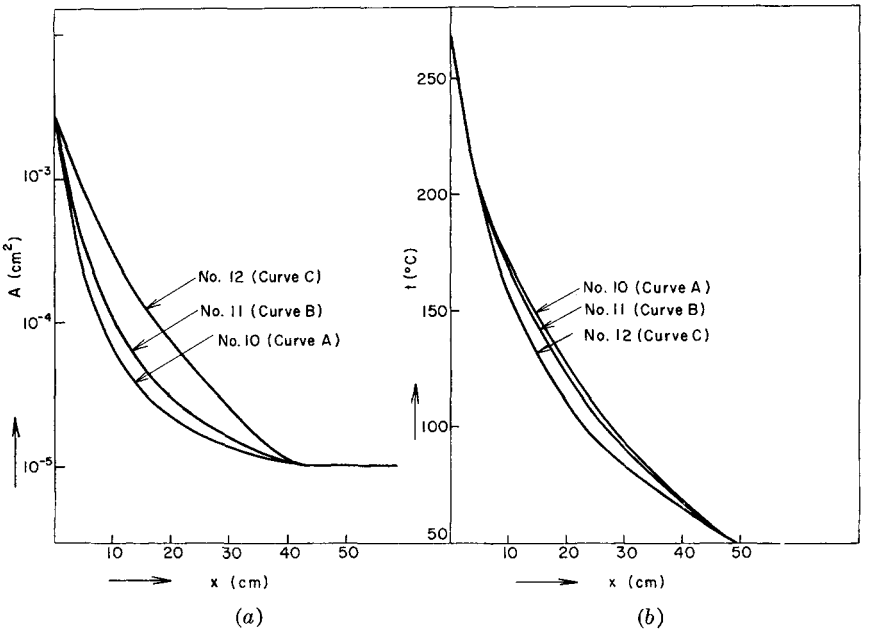

Fig. 11. $A(x)$ and $t(x)$ calculated at various tensile viscosities $\beta(t)$. See Fig. 4.

Theoretical $A(x)$ and $t(x)$ curves consistently agree well with experimental points, although temperature curves show some deviation from experimental values near the spinneret.

Changes in the intrinsic viscosity $[\eta]$ of the yarns taken up do not seem to affect the $A(x)$ and $t(x)$ to any great extent. In Figure 7, for instance, raising the spinneret temperature from 240 to 270°C. resulted in a decrease in the yarn intrinsic viscosity $[\eta]$ from 1.32 to 1.08, but the experimental points in these figures do not reflect such a change. We will discuss this topic further in relation to Figure 11.

The Barus effect, when excessive, causes experimental $A(x)$ values to deviate from the theoretical curve. Experimental points for curve 9 in

Figure 10*a*, for example, exhibit a prominent Barus effect as a result of the large rate G of polymer flow.

The following paragraphs discuss the way in which the spinning conditions affect the theoretical $A(x)$ and $t(x)$ values.

Changes in Tensile Viscosity $\beta(t)$, Density ρ, and Specific Heat C_p

Curves 10, 11, and 12 in Figure 11 correspond to curves A, B, and C in Figure 4. Conditions other than the $\beta(t)$ are identical. It is evident that the steeper the $\log \beta$ versus $1000/(t + 273)$ curve, the closer the $A(x)$ curve to the $x = 0$ line. In other words, the larger the activation energy of the polymer, the more quickly the filament thins below the spinneret. Such changes in $\beta(t)$, however, do not greatly affect the $t(x)$ curve.

On the other hand, when $\beta(t)$ values are increased or decreased by a certain fixed percentage, the $\log \beta$ versus $1000/(t + 273)$ curve is shifted in the vertical direction, but it does not change the $A(x)$ and $t(x)$ curves in any way. It merely changes the spinning tension F in proportion to the change in β. This presumably is the reason why, in Figure 7, changes in yarn intrinsic viscosity $[\eta]$ do not affect the $A(x)$ and $t(x)$ to appreciable extent. $[\eta]$ may have changed the value of β by a fixed percentage.

It can be reasoned from eq. (24) that, other conditions being equal, the filament tension F follows the proportionality:

$$F \propto \beta(270)\rho^{-1}C_p^{-1}v_y^{0.334} \tag{25}$$

and the gradient (dA/dx) of the $A(x)$ curve follows

$$(dA/dx) \propto C_p^{-1}v_y^{0.334}AG^{-1} \tag{26}$$

Polyesters have a greater $\beta(t)$ and a smaller C_p than polypropylene. Therefore, other conditions such as A_N and A_w being equal, polyesters should develop larger spinning tensions F, and the distance required to reach solidification should be smaller than for polypropylene.

Effects of Changes in Nozzle Diameter

Figure 12 shows that increasing the nozzle diameter with no change in take-up speed or take-up denier moves the $A(x)$ and $t(x)$ curves in the x direction and increases the filament tension F.

Effects of Changes in Take-up Speed

Increasing the take-up speed while maintaining a constant take-up denier moves both $A(x)$ and $t(x)$ curves away from the $x = 0$ line, but changes F very little.

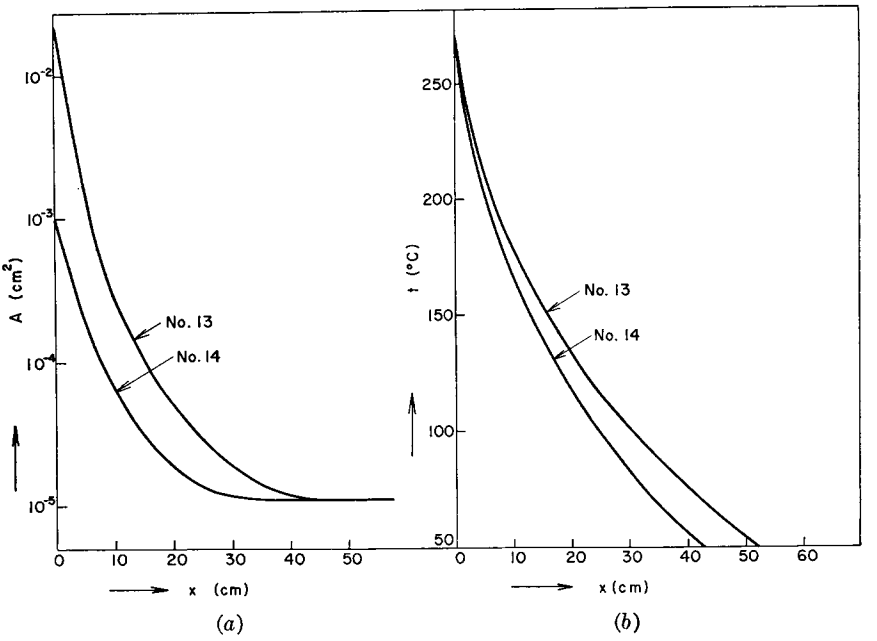

Fig. 12. $A(x)$ and $t(x)$ calculated at different nozzle diameters.

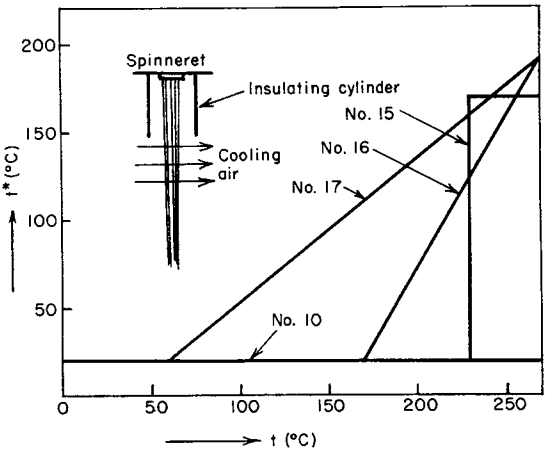

Fig. 13. Fictitious air temperature t^* that represents the effect of three different insulating cylinders placed below the spinneret. Fig. 14 gives the resulting $A(x)$ and $t(x)$. Air speed v_y is assumed zero whenever t^* is above 20°C.

Effects of Placing an Insulating Cylinder below the Spinneret

In computing curves 15, 16, and 17 in Figure 14 it is assumed that an insulating cylinder is placed immediately below the spinnerent; air temperatures inside the insulating cylinder are as shown in Figure 13; air speed v_y inside the cylinder is zero; and outside the cylinder both t^* and v_y are

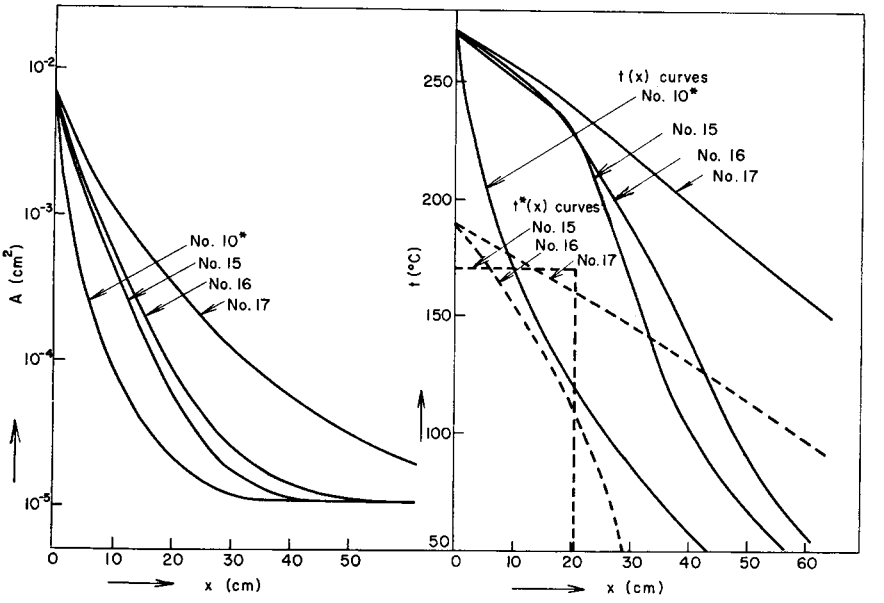

(a) (b)

Fig. 14. $A(x)$ and $t(x)$ under four different $t^*(x)$ curves showing the effects of placing insulating cylinders below the spinneret. No. 10* is a control. The t^* values are given initially as shown in Fig. 13.

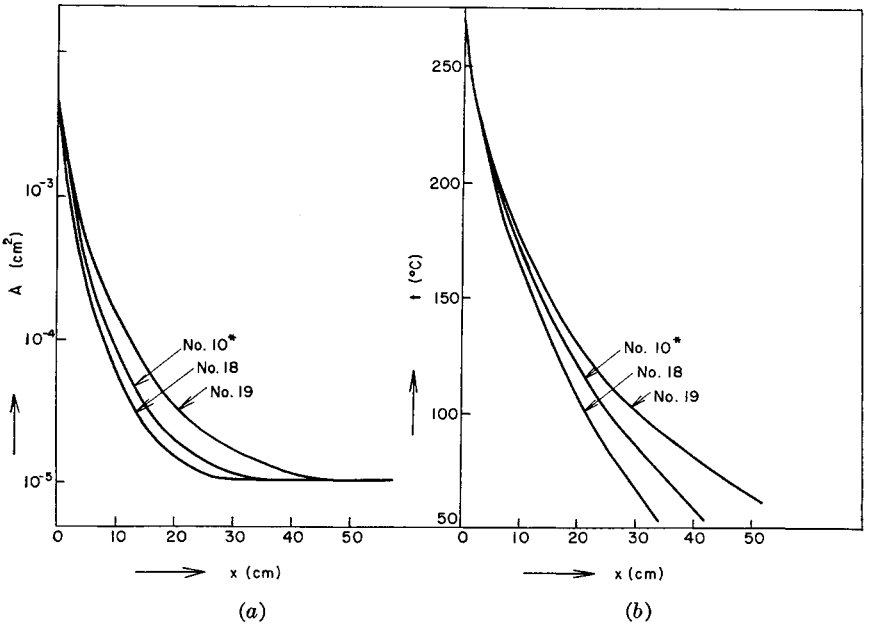

(a) (b)

Fig. 15. $A(x)$ and $t(x)$ curves for three different air temperature values: $t^* = 0$, 20, and 50°C.

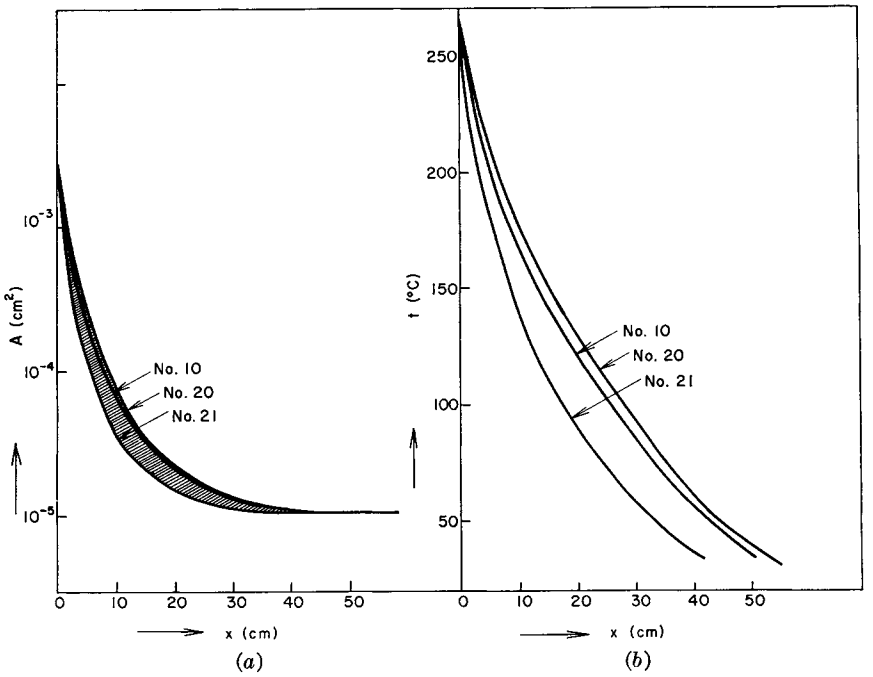

Fig. 16. $A(x)$ and $t(x)$ curves for three different air speeds: v_y = 20, 30, and 120 cm./sec.

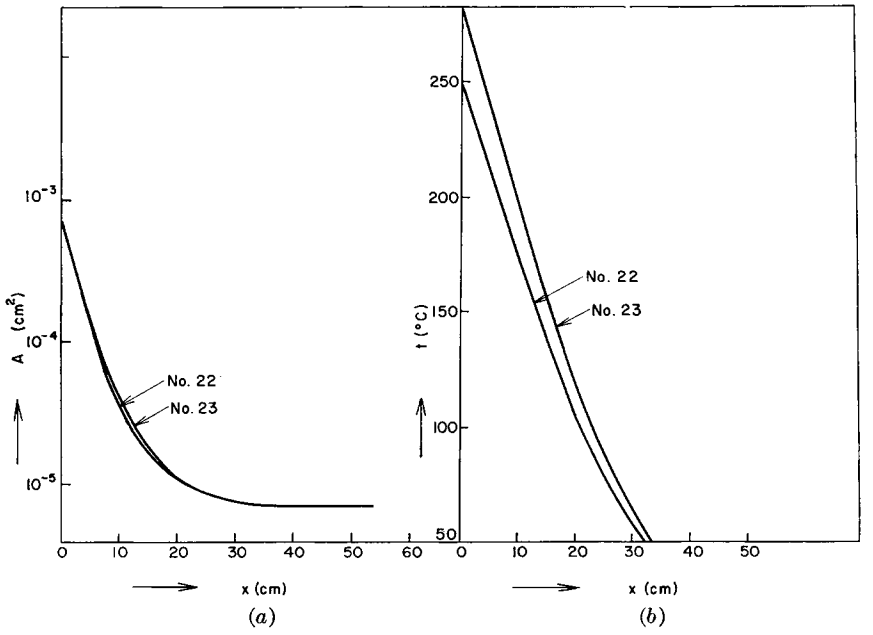

Fig. 17. $A(x)$ and $t(x)$ curves calculated at two different spinneret temperatures: t_N = 250 and 280°C.

constant as in other $A(x)$ and $t(x)$ curves. Thinning and cooling of the polymer filament are delayed by the use of an insulating cylinder, and the delay increases with the cylinder length.

Effects of Changing Air Temperature t^*

Lowering the air temperature t^* makes the filament thin and cool more quickly and increases the filament tension F (Fig. 15).

Effects of Changing Air Speed v_y

Increasing the speed v_y of cooling air is similar in consequences to lowering the air temperature t^* (Fig. 16). It makes the filament thin and cool more quickly, increases tension F, and decreases the polymer holdup within the spinning chamber.

Effects of Changes in Spinneret Temperature t_N

As Figures 7, 8, and 17 show, raising the spinneret temperature t_N without changes in other spinning conditions shifts the $t(x)$ curve upward and decreases the filament tension F. The $A(x)$ curve, however, is affected very little.

Effects of Changing the Polymer Flow Rate G

Curves for polypropylene are shown in Figure 10 and those for polyester in Figure 18. Increasing the nozzle output or the polymer flow rate G at a constant take-up speed greatly increases the distance required for the fila-

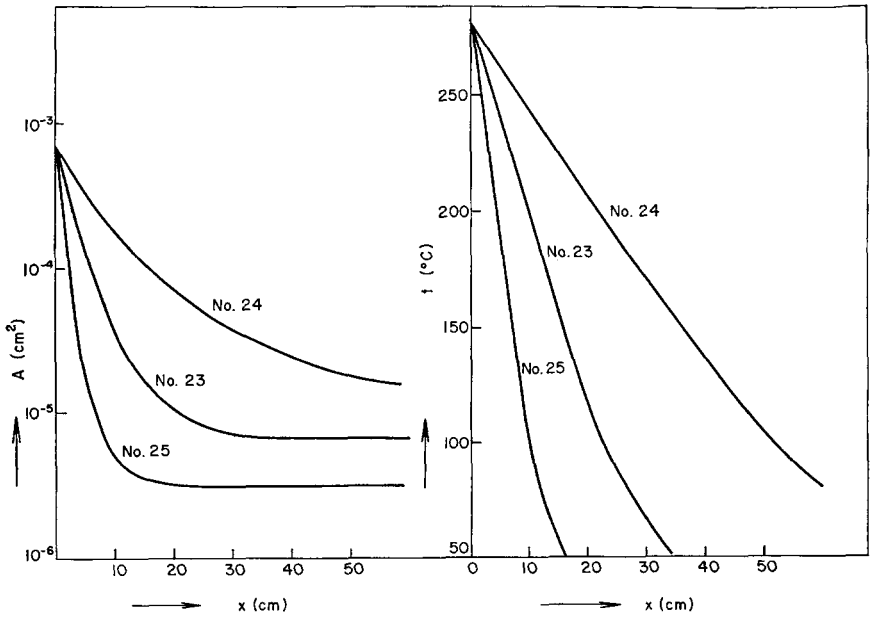

Fig. 18. $A(x)$ and $t(x)$ curves for three different polymer flow rates.

ment to solidify. Filament tension F, however, remains almost unchanged.

When G becomes excessively large, the theoretical $A(x)$ and $t(x)$ curves start to deviate from experimental values because (*a*) the Barus effect becomes prominent, (*b*) the temperature distribution across the filament becomes significant, and (*c*) and filament tension F becomes dependent on position x (see Fig. 37).

CORRELATION BETWEEN YARN QUALITIES AND STEADY-STATE SOLUTIONS

Commercial, mass-produced polyester filament yarns are in almost perfectly amorphous state when taken up on a melt-spinning machine. Therefore, the major factor determining their properties is the molecular orientation. Polypropylene filament yarns, on the other hand, crystallize very quickly in melt spinning, making the cystallinity an important factor as well as the molecular orientation.

According to Thompson[7] and Nishiumi[8] the birefringence Δn increases very quickly as the polymer filament approaches the end of thinning in melt spinning. To this date, however, no published theory has enabled to derive yarn Δn quantitatively from the $A(x)$ and $t(x)$ curves. Here we accept the assumptions that (*1*) molecular orientation develops abruptly at or immediately before the solidification point and (*2*) as soon as the filaments solidify the Δn developed is permanently set for the yarns taken up.

According to the theory of rubber elasticity, the tensile stress $(F/A)c$ acting on the filament at the solidification point is related to the elongation λ of molecules by

$$(F/A)c = k(t + 273)\mu(\lambda^2 - 1/\lambda) \tag{27}$$

where μ is the effective number of molecular chains per unit volume and k is the Boltzmann constant. λ in turn is related to birefringence Δn by the formula

$$\Delta n = \mu M(\lambda^2 - 1/\lambda) \tag{28}$$

where M is a constant determined by the optical properties of the molecule. It follows then that

$$\Delta n = [M/k(t + 273)](F/A)c \tag{29}$$

Yarn birefringence Δn is, therefore, expected to be directly proportional to the tensile stress $(F/A)c$ at the solidification point. $(F/A)c$ in turn is approximately equal to the tensile stress (F/A_w) at the take-up roll.

Yarn crystallinity is expected to depend on the two elements: (*1*) speed of crystallization as a function of polymer temperature t; (*2*) length of time the polymer spends in the particular temperature range having highest crystallization speed.

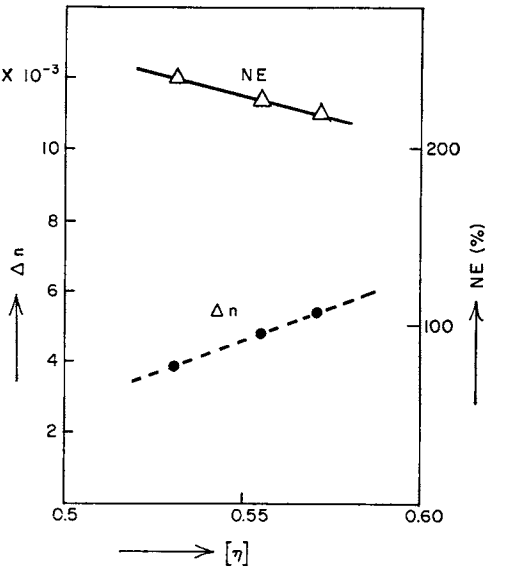

Fig. 19. Measured yarn birefringence Δn and NE values vs. $[\eta]$ for polyester yarns.

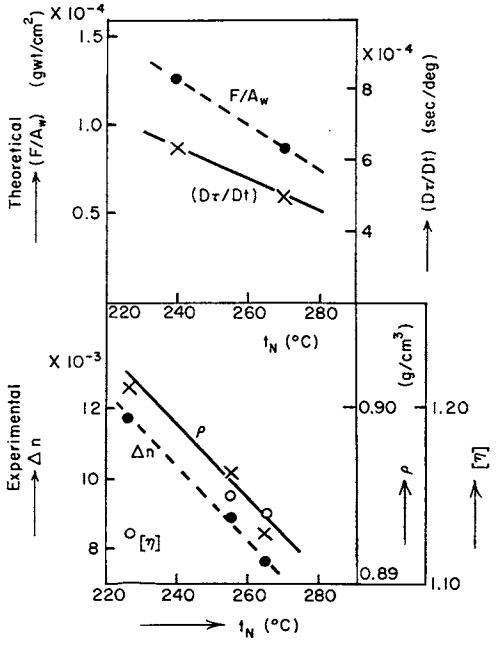

Fig. 20. Changes in calculated tensile stress F/A_w and cooling time $D\tau/Dt$ with spinneret temperature t_N and corresponding changes in yarn Δn and density ρ for polypropylene yarns.

Once a particular polymer type is specified the first of the above two elements becomes fixed, leaving the second element affected by spinning conditions. The second element can be expressed quantitatively by the

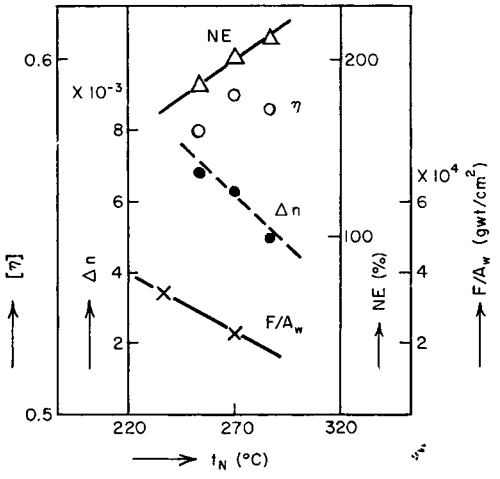

Fig. 21. Effects of spinneret temperature t_N on measured yarn Δn, NE, and calculated F/A_w at constant $[\eta]$ for polyester yarns.

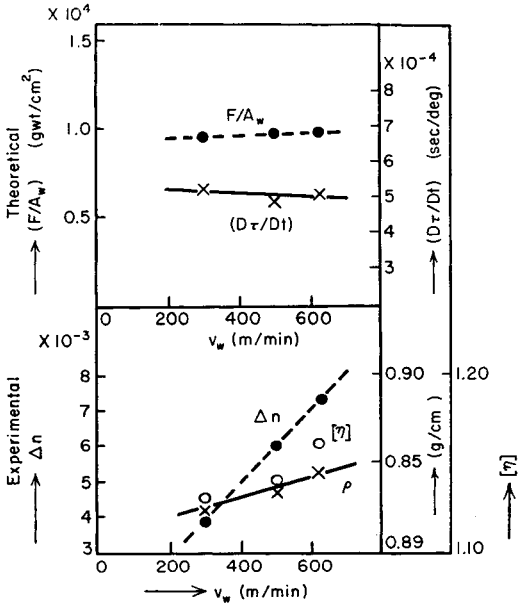

Fig. 22. Effects of take-up speed v_w on calculated tensile stress F/A_w, calculated cooling time $D\tau/Dt$, measured yarn birefringence Δn, and measured yarn density ρ for polypropylene yarns.

length of time the polymer filament requires to cool by 1°C. as given in eq. (30).

$$(D\tau/Dt) = (\rho A/G)(dx/dt)_{t_{opt}} \tag{30}$$

For simplicity we hereafter call $(D\tau/Dt)$ the cooling time. In eq. (30) t_{opt} is the polymer temperature at which the crystallization speed is highest.

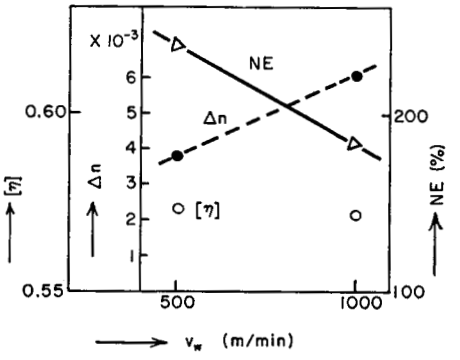

Fig. 23. Effects of take-up speed v_w on measured yarn Δn and NE at constant $[\eta]$ for polyester yarns.

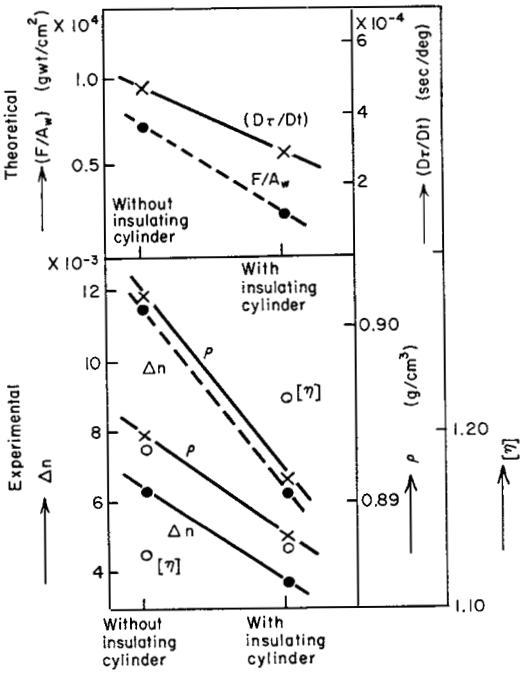

Fig. 24. Calculated tensile stress F/A_w, calculated cooling time $D\tau/Dt$, measured yarn Δn, and measured yarn density ρ with and without an insulating cylinder for polypropylene yarns.

Since polypropylene crystallizes very quickly it is difficult experimentally to determine its t_{opt} value accurately. We have found, however, that polypropylene crystallizes much faster at 110°C. than at 120°C. On the other hand, t_{opt} can not be less than 80°C. since at such low temperatures $(D\tau/Dt)$ is known to become practically independent of spinning conditions which in practice greatly affect crystallinity. Polyester filaments which are spun

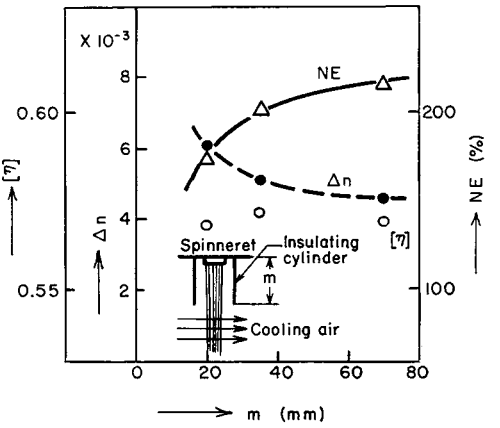

Fig. 25. Changes in measured yarn Δn and NE with changes in the length m of the insulating cylinder at constant $[\eta]$ for polyester yarns.

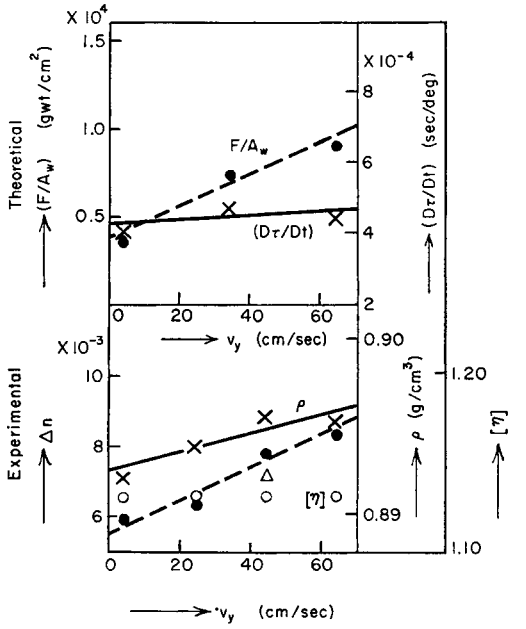

Fig. 26. Changes in calculated tensile stress F/A_w, calculated cooling time $D\tau/Dt$, measured yarn Δn, and measured yarn density ρ with changes in cooling air speed v_y for polypropylene yarns.

from a 90% poly(ethylene terephthalate)–10% poly(ethylene isophthalate) copolymer are assumed to have t_{opt} = 152°C., from data on poly(ethylene terephthalate).

Figures 19–27 show how the experimentally measured birefringence Δn and density of melt-spun yarns change with spinning conditions. Shown in addition to Δn and ρ are tensile stress F/A_w and cooling time $(D\tau/Dt)$ derived from steady-state $A(x)$ and $t(x)$ values. The values designated as NE in these figures are elongation percentages at which necks vanishes from filament yarns cold-drawn at a rate of 400%/min. and at a temperature of 20°C. Spinning conditions other than those mentioned in these figures for polypropylene filament yarns: spinneret temperature t_N, 260°C.; take-up speed, 500 m./min.; take-up denier, 8 den.; cooling air hits the filaments 1.0 cm. below the spinneret; cooling air temperature t^*, 20°C.; cooling air speed v_y, 30 cm./sec.; intrinsic viscosity of pellets $[\eta]$, 1.55.

Spinning conditions for polyester filament yarns are as follows: spinneret temperature t_N, 270°C.; take-up speed, 750 m./min.; take-up denier, 8.5 den.; cooling air hits the filaments 2.0 cm. below the spinneret; cooling air temperature t^*, 20°C.; cooling air speed v_y, 30 cm./sec.

In planning these experiments, care was taken to make the yarn intrinsic viscosity $[\eta]$ remain as constant as possible. In Figure 27, for example, the number of filament ends is changed as well as the take-up denier so as to make the polymer stay in the extruder for the same length of time. As a result, heat degradation in the spinning machine remains unchanged, and consequently the yarn $[\eta]$ remains approximately constant.

$[\eta]$ of polypropylene yarns was kept in the range $[\eta]$ = 1.15–1.20 (except for the first series of experiments), since the crystallization speed is most sensitive to changes in spinning conditions when $[\eta]$ stays in this range.

Effects of Changes in the Yarn Intrinsic Viscosity

Figure 19 shows that birefringence Δn of polyester yarns increases with the intrinsic viscosity $[\eta]$. This is in agreement with the theoretical reasoning discussed before; that is to say, an increase in $[\eta]$ increases tensile viscosity β, yarn tension F, tensile stress F/A_w and finally birefringence Δn.

Effects of Changes in Spinneret Temperature t_N

Figure 20 shows the effects of raising the spinneret temperature t_N in melt spinning of polypropylene filament yarns. Theory agrees with experimental results in that the measured Δn decreases with calculated F/A_w and the measured yarn density ρ decreases with the calculated cooling time $(D\tau/Dt)$. Here the extruder output is adjusted in such a way to maintain an approximately constant yarn $[\eta]$. Otherwise, yarn $[\eta]$ will tend to decrease with increasing t_N, making it impossible to separate the effects of t_N.

Figure 21 shows that polyester filament yarns are similar in trends to polypropylene yarn.

Effects of Changes in the Take-up Speed at Constant Take-up Denier

Theory (Fig. 22*a*) does not agree with experimental results (Fig. 22*b*), in that both Δn and ρ values increase with the take-up speed while F/A_w and $(D\tau/Dt)$ values remain almost unchanged. We have not succeeded in giving reasonable explanation to this discrepancy.

Figure 23 shows that Δn of polyester yarns increases with the take-up speed.

Effects of Placing an Insulating Cylinder below the Spinneret

An insulating cylinder placed below the spinneret has the effect of maintaining high air temperatures and nearly zero air speeds inside the cylinder. Figure 24 shows that using an insulating cylinder reduces all four values, the calculated F/A_w and $D\tau/Dt$ and experimentally measured Δn and ρ. The theoretical prediction is, therefore, considered to be in agreement with the experimental results.

Temporarily delaying the cooling of polymer filament by placing an insulating cylinder to give in less crystalline yarns sounds somewhat paradoxical. This apparent paradox comes from the fact that the cooling time $D\tau/Dt$ is equal to the ratio of dt/dx over the yarn speed v as eq. (30) shows. Since the insulating cylinder delays cooling it allows the filament

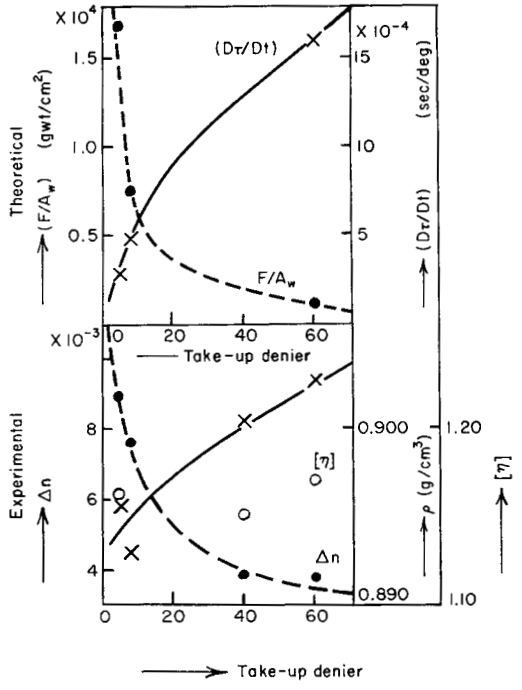

Fig. 27. F/A_w, $D\tau/Dt$, Δn, and ρ vs. take-up denier for polypropylene yarns.

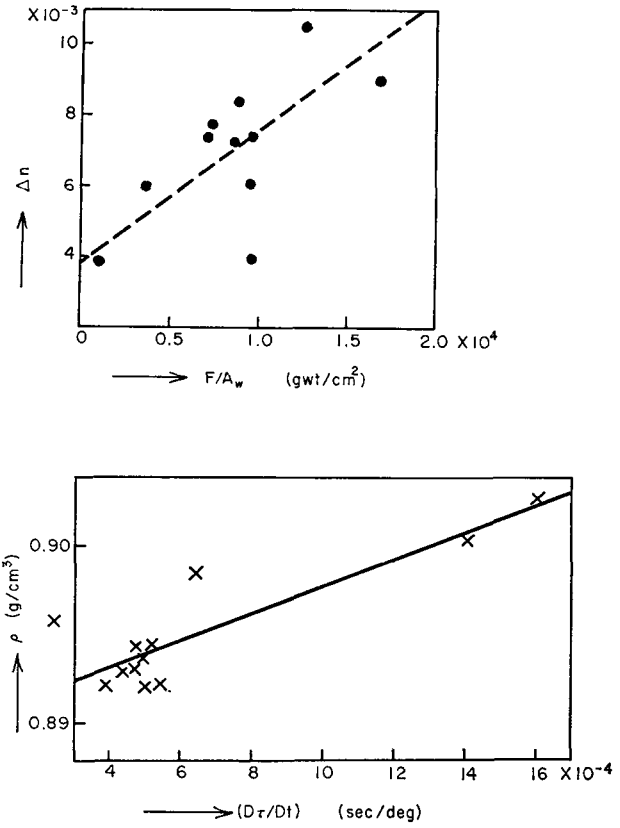

Fig. 28. Correlation between Δn (experimental) and F/A_w (theoretical) and between ρ (experimental) and $D\tau/Dt$ (theoretical) for polypropylene yarns. Summary of Figs. 20, 22, 24, 26, and 27.

to thin to gain a high running speed v by the time the filament is eventually cooled to 100°C. This makes the cooling time small, and consequently the yarns are less crystalline.

Effects are similar on polyester yarns, as shown in Figure 25.

Effects of Changes in the Speed v_y of Cooling Air

Theoretically derived F/A_w and $D\tau/Dt$ values agree in trend with experimentally measured Δn and ρ values in that all four values increase with air speed v_y (Fig. 26).

Effects of Changes in the Take-up Denier with the Take-up Speed at Constant v_w

Theoretical prediction agrees in with experimental values, in that F/A_w and Δn increase with take-up denier while $D\tau/Dt$ and ρ decrease with take-up denier (Fig. 27).

The correlations between Δn and F/A_w and between ρ and $D\tau/Dt$ are summarized in Figure 28.

TRANSIENT SOLUTION AND EXPERIMENTAL VALUES

Numerical computation on a digital calculator is the only practical way to solve the fundamental eqs. (18), (19), and (20) for a transient solution.

Among the infinite number of transient solutions the authors chose to solve the following one.

Problem statement: Compute the changes with time in the cross-sectional area A of the filament at the take-up roll after an abrupt increase in the speed v_y of cooling air. It is assumed that at time $\tau = 0$ variables A, t, and v are equal to their respective steady-state values, that A, t, and v are constants at the spinneret, and that v is constant at the take-up roll.

The first step in the problem solution is to linearize eqs. (18), (19), and (20) by replacing the dependent variables with their incremental changes about the steady-state values. Variables A, v, t, v_y, and F are split into their steady-state values A_0, v_0, t_0, v_{y0}, and F_0 plus incremental changes A_1, v_1, t_1, v_{y1} and F_1.

$$t(x,\tau) = t_0(x) + t_1(x,\tau) \tag{31}$$

$$v(x,\tau) = v_0(x) + v_1(x,\tau) \tag{32}$$

$$A(x,\tau) = A_0(x) + A_1(x,\tau) \tag{33}$$

$$v_y(x,\tau) = v_{y0}(x) + v_{y1}(x,\tau) \tag{34}$$

$$F(\tau) = F_0 + F_1(\tau) \tag{35}$$

Incremental changes are then normalized by dividing each by its steady-state values. This defines five new variables.

$$\bar{t}(x,\tau) = t_1(x,\tau)/[t_0(x) - t^*(x)] \tag{36}$$

$$\bar{v}(x,\tau) = v_1(x,\tau)/v_0(x) \tag{37}$$

$$\bar{A}(x,\tau) = A_1(x,\tau)/A_0(x) \tag{38}$$

$$\bar{v}_y(x,\tau) = v_{y1}(x,\tau)/v_{y0}(x) \tag{39}$$

$$\bar{F}(\tau) = F_1(\tau)/F_0 \tag{40}$$

Unlike in the steady-state solutions, yarn tension F is in general an unknown function of time τ rather than an unknown constant. The values of F or $\bar{F}$ are determined during the process of problem solution in such a manner as to satisfy the boundary conditions. In the present problem the boundary condition to be satisfied by making adjustments on $\bar{F}$ is the yarn speed v at the take-up roll.

Another new variable z is defined to replace x.

$$z = \int_0^x [1/v_0(x)]dx \tag{41}$$

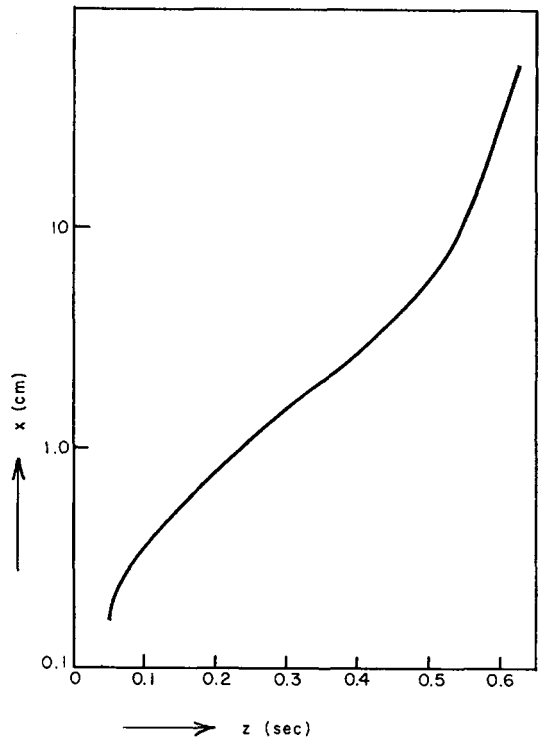

Fig. 29. Position x vs. z for curve 8 of Fig. 10.

z is the duration of time the polymer takes to flow from the spinneret to the $x = x$ position under a steady-state condition. The z versus x relation shown in Figure 29 is that for curve 8 in Figure 10*a* and Table I.

By introducing eqs. (36)–(41) into eqs. (18), (19), and (20) and by neglecting the second-order and higher terms with respect to the new dependent variables we get a set of linearized equations:

$$(\partial \bar{l}/\partial z) + (\partial \bar{l}/\partial \tau) = f_3(z)\bar{A} + f_4(z)\bar{v} - f_5(z)\bar{v} \tag{42}$$

$$(\partial \bar{v}/\partial z) = f_1(z)(\bar{F} - \bar{v} - \bar{A}) + f_2(z)\bar{l} \tag{43}$$

$$(\partial \bar{A}/\partial z) + (\partial \bar{A}/\partial \tau) = -(\partial \bar{v}/\partial z) \tag{44}$$

where

$$f_1(z) = (F_0/\beta_0 A_0) = -(v_0 A_0)(dA_0/dx) \tag{45}$$

$$f_2(z) = -(v_0/A_0)(dA_0/dx)(t_0 - t^*)(-1/\beta_0)(d\beta_0/dt) \tag{46}$$

$$f_3(z) = 2.89 \times 10^{-4} A_0^{-0.833} v_0^{0.334}[1 + (8v_{y0}/v_0)^2]0.833$$
$$= -[(dt_0/dx)v_0/(t_0 - t^*)]0.833 \tag{47}$$

$$f_4(z) = -\frac{(dt_0/dx)v_0}{t_0 - t^*} 0.666 \frac{1 + 1.5(8v_{y0}/v_0)^2}{1 + (8v_{y0}/v_0)^2} \tag{48}$$

$$f_5(z) = -\frac{(dt_0/dx)v_0}{t_0 - t^*} 0.333 \frac{(8v_{y0}/v_0)^2}{1 + (8v_{y0}/v_0)^2} \tag{49}$$

Shown in Figure 30 are coefficients $f_1(z)$ through $f_5(z)$ derived from the $A_0(x)$ and $t_0(x)$ values for curve 8 of Table I and Figure 10*a*.

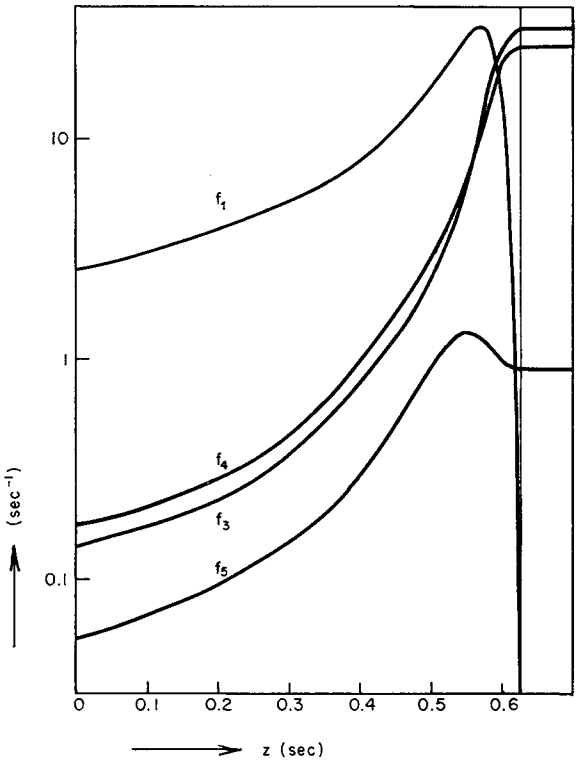

Fig. 30. Coefficients f_1, f_3, f_4, and f_5 vs. z for curve 8 in Fig. 10.

To facilitate numerical computation, eqs. (42), (43), and (44) must be converted into simultaneous difference equations. To do so, coordinates z and τ are divided into evenly spaced discrete values, 0, 1, 2, . . ., i, . . ., 25 and 0, 1, 2, . . ., j, . . ., 80 as shown in Figure 31. $i = 25$ corresponds to the solidification point where the filament cross-section reaches its final take-up value. Difference intervals Δz and $\Delta\tau$ are both set at 0.025 sec. in magnitude.

$$\Delta z = \Delta\tau = 0.025 \text{ sec.} \tag{50}$$

The derivatives with respect to z and τ in eqs. (42)–(44) are then replaced with differences:

$$(\partial\bar{v}/\partial z) \rightarrow [\bar{v}(i,j-1) - \bar{v}(i-1,j-1)]/\Delta z \tag{51}$$

$$(\partial\bar{A}/\partial\tau) \rightarrow [\bar{A}(i,j) - \bar{A}(i,j-1)]/\Delta\tau \tag{52}$$

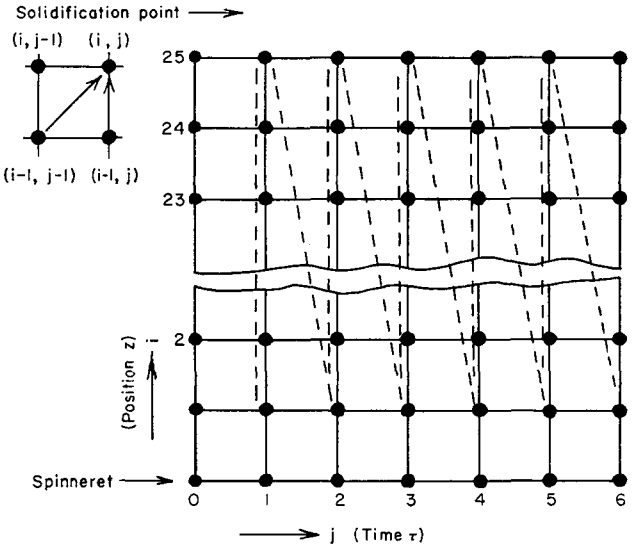

Fig. 31. Discrete coordinates i and j. Sequence of digital computation.

to get a set of simultaneous difference equations

$$\bar{l}(i,j) = f_3(i-1)\Delta z\bar{A}(i-1,j-1) + f_4(i-1)\Delta z\bar{v}(i-1,j-1) + f_5(i-1)\Delta z\bar{v}(i-1,j-1) + \bar{l}(i-1,j-1) \quad (53)$$

$$\bar{v}(i,j-1) = f_1(i-1)\Delta z[\bar{F}(j-1) - \bar{A}(i-1,j-1)] + [1 - f_1(i-1)\Delta z]\bar{v}(i,j-1) + f_2(i-1)\Delta z\bar{l}(i-1,j-1) \quad (54)$$

$$\bar{A}(i,j) = \bar{A}(i-1,j-1) - \bar{v}(i,j-1) + \bar{v}(i-1,j-1) \quad (55)$$

Boundary conditions given by the problem statement are as follows.
Initial conditions:

$$\bar{l}(i,0) = \bar{v}(i,0) = \bar{A}(i,0) = 0 \quad (56)$$

Conditions at the spinneret:

$$\bar{l}(0,j) = \bar{v}(0,j) = \bar{A}(0,j) = 0 \quad (57)$$

Condition at the solidification point:

$$\bar{v}(25,j) = 0 \quad (58)$$

Changes in the speed of cooling air:

$$\bar{v}_y(i,j) = 1 \quad (59)$$

As the definitions in eqs. (36)–(40) show, $\bar{v} = 0$ means that v is equal to its steady-state value v_0.

The solution of eqs. (53), (54), and (55) that satisfies the above boundary conditions is computed by the sequence shown diagrammatically in Figure

32. In this system, values of $\bar{A}$, $\bar{v}$, and $\bar{t}$ along lines OD and OE in Figure 31 are given by eqs. (56) and (57). Equations (53) and (55) moves the computations from the $(i-1,j-1)$ point to the (i,j) point while eq. (54) moves the computation upwards from the $(i-1,j-1)$ point to the $(i,j-1)$ point. By using these equations repetitively the computation proceeds along the zig-zag path shown in Figure 31. Filament tension $\bar{F}(j-1)$ is computed column by column taking advantage of the convenient relation

$$\partial\bar{v}(25,j-1)/\partial\bar{F}(j-1) \doteq 1 \tag{60}$$

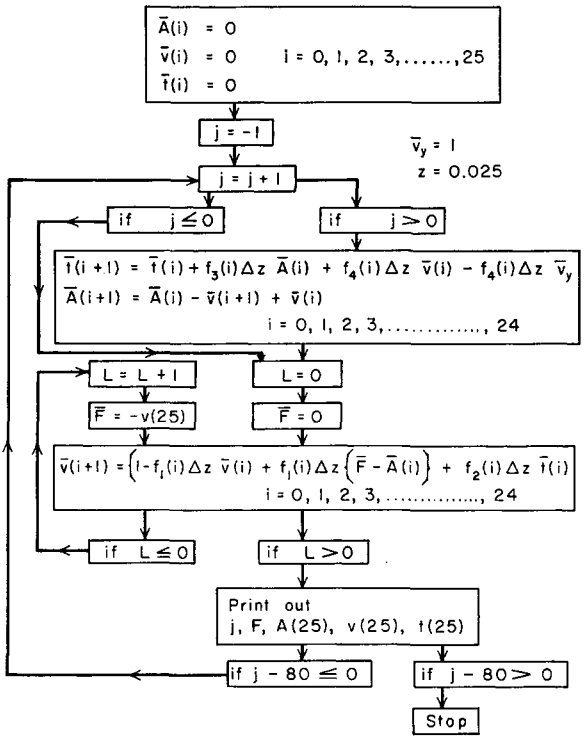

Fig. 32. Flow diagram for digital computation of transient solution. Input signal is a stepwise change in the speed v_y of cooling air.

and eq. (54) in such a way to satisfy eq. (58). This involves computing $\bar{v}(1, j-1) \ldots \bar{v}(25,j-1)$ twice. In the first trial, $\bar{v}(25, j-1)$ is computed with the $\bar{F}(j-1)$ in eq. (54) assumed zero. Then eq. (60) is used to determine the value of $\bar{F}(j-1)$ that satisfies eq. (58). Computation is repeated with the use of the newly found $\bar{F}(j-1)$ value.

Computations were carried out with an IBM 1401 machine with the results shown in Figure 33. $\bar{F}$ and $\bar{A}$ in Figure 33 are per cent changes in filament tension and filament cross-section after an abrupt increase by 1% in the speed of cooling air. Time scale is in seconds.

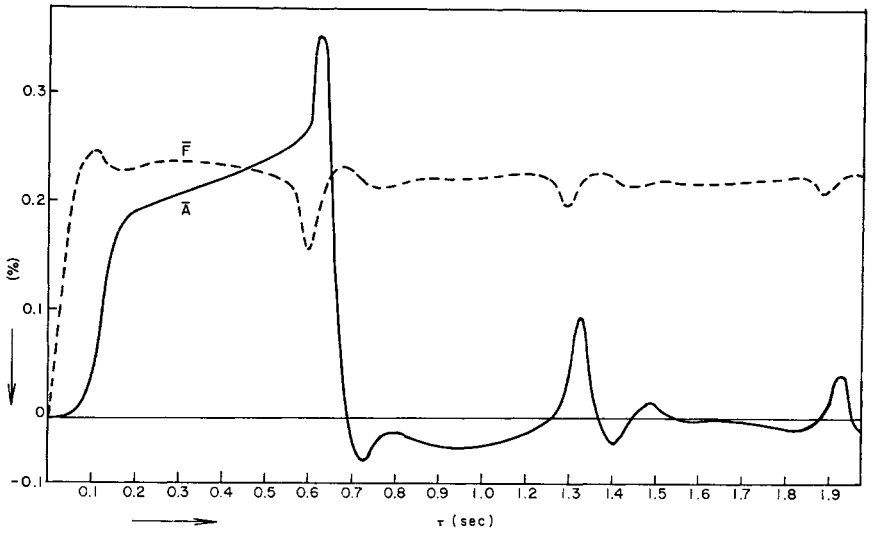

Fig. 33. Transient solution of eqs. (42), (43), and (44), showing per cent change in filament cross-section A_w and filament tension F after a sudden 1% increase in cooling air speed.

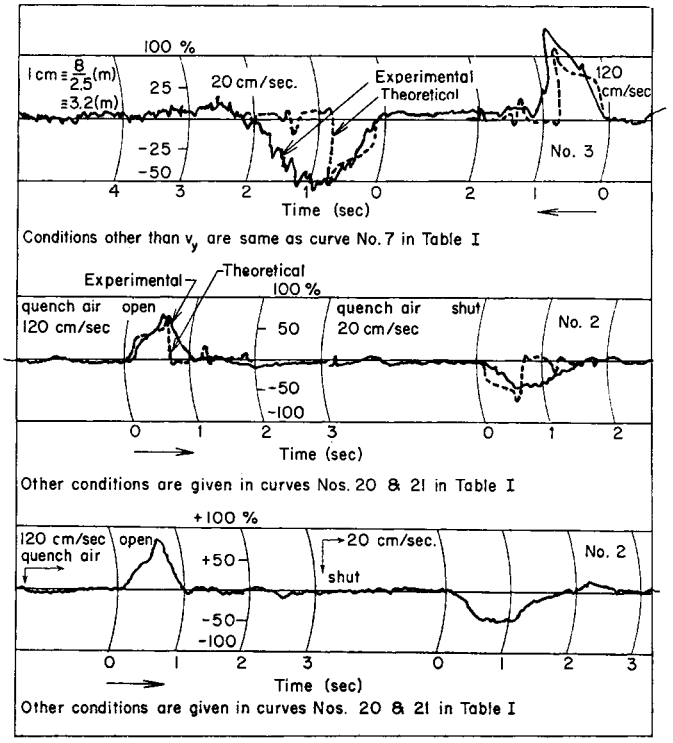

Fig. 34. Experimental results corresponding to the theoretical curve in Fig. 33.

Figure 34 shows experimental results that corresponds to the theoretical curves in Figure 33. The broken curves are theoretical $\bar{A}$ curves transcribed from Figure 33. In these experiments, cooling air speed is changed abruptly from 20 cm./sec. to 120 cm./sec. and a few seconds later back to 20 cm./sec. The thickness of the polypropylene yarn thus produced is then measured on an Uster evenness tester (Zellweger Ltd.).

Spinning conditions other than the air speed are same as in runs 7 and 8 in Table I. For all their nonlinearity the experimental curves agree fairly well with theoretical curves.

Thus, a filament yarn becomes temporarily thick after a sudden increase in the cooling air speed. A qualitative explanation for this thickening is given by the steady-state $A(x)$ curves shown in Figure 16. Increasing

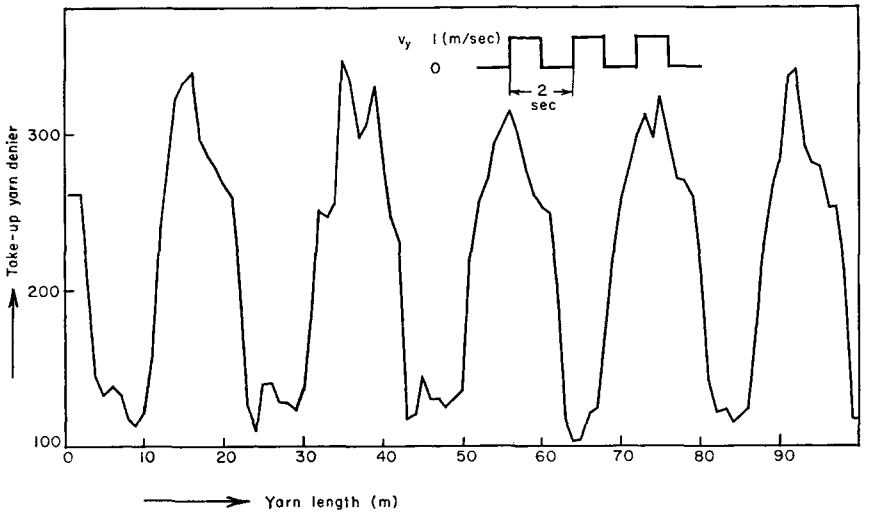

Fig. 35. Oscillation in yarn denier produced by periodically shutting off cooling air; polypropylene yarn.

the cooling air speed from 20 cm./sec. to 120 cm./sec. changes the steady-state $A(x)$ from the top curve to the bottom curve. The resultant decrease in polymer hold-up below the spinneret shown as the shaded portion in Figure 16*a* must be discharged downwards. This discharge accounts for the temporary thickening of the filament yarn.

Figures 29 and 33 show that, in theory, the length of time the filament is thick is equal to the residence time, i.e., the time the filament takes to flow from the spinneret to the solidification point. It follows then that the melt-spinning system has a period of oscillation equal to twice the above residence time. As Figure 35 shows, a filament yarn being melt-spun does develop a severe oscillation in its thickness when the cooling air is shut off periodically at regular intervals. The oscillation shown in Figure 35 has a period of 2 sec. or 17 m. in yarn length which is some 50% more than the theoretical period.

SUMMARY AND COMMENTS

There have been many studies on melt spinning in which the correlations between spinning conditions and yarn qualities are discussed, but few of them have analyzed theoretically the mechanism of melt spinning which account for such correlations. In an effort to fill this gap, we introduced in this study a set of simultaneous differential equations which simulate the filament being melt spun. The cross-section $A(x)$, temperature $t(x)$, and tension F have been derived as steady-state solutions to the above equations. F/A_w and $(D\tau/Dt)$ values derived from above A, t, and F values have been found to show fairly good correlation with experimentally measured yarn qualities Δn and ρ.

To make possible a truly quantitative derivation of yarn qualities, however, further refinements will be required on the mathematical model and experimental techniques. These will be (*1*) more accuracy in the measurement of β values, (*2*) better control of cooling air flow so that h can be predicted more accurately, (*3*) consideration of the temperature gradient across the filament, (*4*) more studies on the dependence of filament tension on air resistance, (*5*) better theories on the effects of $A(x)$ and F values on birefringence Δn, (*6*) more accurate data on the temperature dependence of crystallization speed.

It is well known that fluctuations in the cooling air speed cause yarn weight variations. A theoretical interpretation of this phenomenon has been obtained by solving the fundamental equations (18), (19), and (20) for a transient solution and comparing the results with experimental results. It has been found that changes in air speed produce yarn weight variations through changes in the coefficient h of heat transfer rather than in a direct mechanical manner.

APPENDIX

Dependence of Filament Tension F on Position x

In deriving eq. (2), Part I, the authors disregarded the air resistance as having negligible influences on filament tension F. However, it was since found that air resistance does become significant at times as Thompson points out.[7] On account of this, we measured the resistance exerted by air stream flowing parallel to a single wire 0.2 mm. in diameter. The resistance f per centimeter wire length shown in Figure 36 is approximated by the formula

$$(fg/2\rho FRv^2) = 1.94\ \mathrm{Re}^{-0.81} \tag{61}$$

where Re is Reynolds number, ρ, is the density of air, and R is the filament radius; f is, therefore,

$$f = 0.55 \times 10^{-6} G^{1.19} \rho^{-1.19} A^{-1.10} \tag{62}$$

Equation (2), Part I, should then be

$$F = F_w - G(v_w - v)/g + \int_x^{x_w} \rho A dx - 0.55 \times 10^{-6} G^{1.19} \int_x^{x_w} \rho^{-1.19} A^{-1.10} dx \quad (63)$$

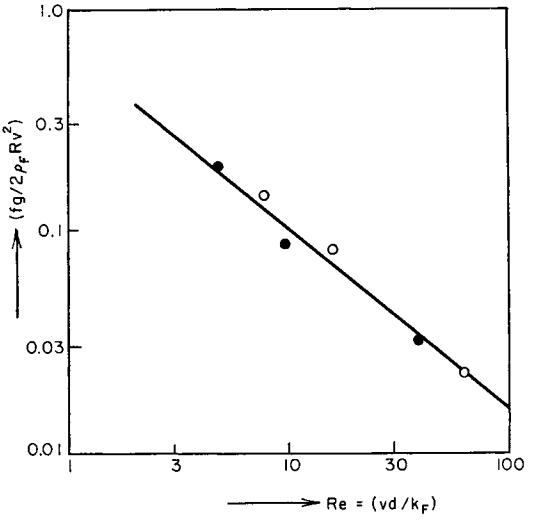

Fig. 36. Resistance force f per centimeter exerted by air stream flowing parallel to a 0.2-mm. wire.

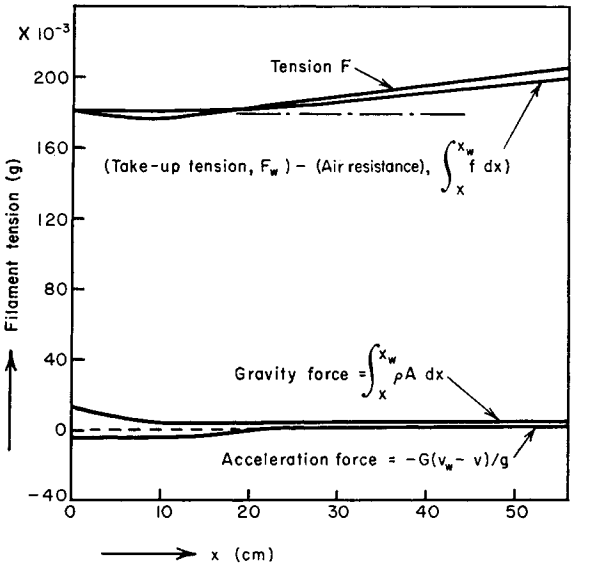

Fig. 37. Filament tension F vs. position x for curve 8 of Fig. 10 calculated by using eq. (63).

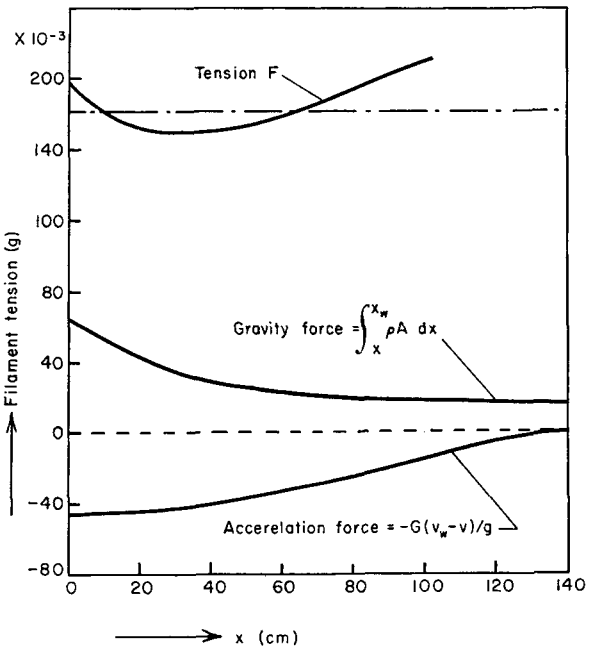

Fig. 38. Filament tension F vs. position x for curve 9 of Fig. 10 calculated by using eq. (63).

where F_w is the take-up tension and v_w is the take-up speed. The second and the third terms are forces of acceleration and gravity. By applying eq. (63) to curves 8 and 9 of Figure 10 we get filament tension F and its four components as shown in Figures 37 and 38. In Figure 37, where the yarn denier is 8, F is nearly independent of position x as has been assumed in the text; in Figure 38, however, where the yarn denier is 60, F varies considerably with x.

Air resistance working on a filament yarn can be measured by measuring tensions at two different positions along the yarn, one at the take-up roll and the other 1 m. below the spinneret, and taking the difference between the two measurements. Air resistance measured in this manner is in most cases less than half the value predicted by eq. (62) based on single wire experiments. A number of filaments running close together seems to reduce air resistance by generating a downward air current.

The authors wish to thank Mitsuyasu Kageyama and Takashi Uyeyama for their cooperation in computations.

References

1. S. Kase and T. Matsuo, *J. Polymer Sci. A*, **3**, 2541 (1965).
2. W. H. McAdams, *Heat Transmission*, 3rd Ed., McGraw-Hill, New York, 1954, p. 259.
3. A. C. Simmons, *Trans. A.I.Ch.E.*, **38**, 613 (1942).
4. L. F. G. Mueller, *Phil. Mag.*, [7] **3**, 81 (1927).

5. Y. Sano and S. Nisikawa, *Kagaku Kogaku* (*Chemical Engineering*), **28**, 275 (1964).
6. C. W. Smith and M. Dole, *J. Polymer Sci.*, **20**, 37 (1956).
7. A. B. Thompson, *Fiber Structure*, Butterworths, London, 1963, p. 485.
8. S. Nishiumi, *J. Textile Mach. Japan*, **18**, 174 (1965).

Résumé

Au début de ce manuscrit, les auteurs formulent les dynamiques du fillage à l'état fondu en introduisant un ensemble d'équations fondamentales qui consistent en des équations balance de chaleur, de force et de matériaux. Certaines solutions stationnaires sont également données. Des solutions additionnelles stationnaires correspondant aux différents conditions de fillage pour des polyesters et des filaments de polypropylène montrent un bon accord avec les résultats expérimentaux. Ces solutions stationnaires qui fournissent la section transversale du filament $A(x)$ et la température du filament $t(x)$ en fonction de la position x sont reliées aux qualités du film: la densité du film et la biréfringence, la cristallinité et l'orientation moléculaire sont reliées respectivement à la vitesse de refroidissement du polymère à 100°C et à la tension maximum $F/A(w)$ agissant sur les filaments. Une solution provisoire des équations fondamentales évaluées sur une machine IBM 1401 montre que la section transversale du filament A à un pic transitoire important après une augmentation graduelle de la vitesse v_y de l'air de refroidissement. Ceci s'accorde bien avec les expériences. C'est rour quoi les équations fondamentales clarifièn la relation dynamique entre la vitesse de l'air de refroidissement et la variation en poids du filaments.

Zusammenfassung

In der ersten Mitteilung haben die Autoren die Dynamik des Schmelzspinnverfahrens durch Einführung einer Reihe fundamentaler Gleichungen, nämlich der Gleichungen für die Wärme-, Kräfte- und Stoffbilanz, beschrieben. Es werden einige Lösungen für den stationären Zustand angegeben. Weitere stationäre, einer Reihe verschiedener Spinnbedingungen für Polyester und Polypropylenfädengarne entsprechende Lösungen zeigen alle gute Übereinstimmung mit den Versuchsergebnissen. Diese Lösungen für stationäre Bedingungen beschreiben den Fadenquerschnitt $A(x)$ und die Fadentemperatur $t(x)$ als Funktion der Lage x, stehen in Korrelation zu Garneigenschaften: Garndichte und -doppelbrechung, Kristallinität und Molekülorientierung und zeigen ausserdem eine Korrelation zur Abkühlungsgeschwindigkeit des Polymeren bei 100°C und zur maximalen, auf den Faden wirkenden Zugspannung $(F/A)_W$. Eine auf einer IBM 1401 berechnete Lösung der Grundgleichungen für instationäre Bedingungen zeigt, dass der Fadenquerschnitt A an der Aufnahmerolle nach schrittweiser Zunahme der Kühlluftgeschwindigkeit v_y ein grosses instationäres Maximum bildet. Das stimmt mit den Versuchen recht gut überein. Die Grundgleichungen geben daher eine Klärung der dynamischen Beziehungen zwischen Kühlluftgeschwindigkeit und Änderungen des Garngewichtes.

Received July 8, 1966
Prod. No. 1455